Title: Liquid-liquid phase separation and viscosity in biomass burning organic aerosol and climatic impacts

Authors: Florence K. A. Gregson[1], Nealan G. A. Gerrebos[1], Meredith Schervish[2], Sepehr Nikkho[1], Elijah G. Schnitzler[3], Carley Schwartz[4], Christopher Carlsten[4], Jonathan P. D. Abbatt[5], Saeid Kamal[1], Manabu Shiraiwa[2], Allan K. Bertram[1,*]

Author Affiliations:

1. **Department of Chemistry, University of British Columbia, Vancouver, V6T 1Z1, BC, Canada**
2. **Department of Chemistry, University of California, Irvine, CA 92697, USA**
3. **Department of Chemistry, Oklahoma State University, Stillwater, OK 74078, USA**
4. **Department of Medicine, Division of Respiratory Medicine, University of British Columbia, V5Z 1M9, BC, Canada**
5. **Department of Chemistry, University of Toronto, Toronto, M5S 3H6, ON Canada**

Email: bertram@chem.ubc.ca

Keywords: Biomass burning, phase behavior, viscosity, brown carbon, heterogeneous reaction kinetics

Abstract

Smoke particles generated by burning biomass consist mainly of organic aerosol, referred to as biomass-burning organic aerosol (BBOA). BBOA influences the climate by scattering and absorbing solar radiation or acting as nuclei for cloud formation. The viscosity and the phase behavior (i.e. the number and type of phases present in a particle) are properties of BBOA that are expected to impact several climate-relevant processes but remain highly uncertain. We studied the phase behavior of BBOA using fluorescence microscopy, and showed that BBOA particles comprise two organic phases (a hydrophobic and a hydrophilic phase) across a wide range of atmospheric relative humidity (RH). We determined the viscosity of the two phases using a photobleaching method, and showed that the two phases possess different RH-dependent viscosities. The viscosity of the hydrophobic phase is largely independent of the RH from 0 to 95%. For temperatures less than 230 K, the hydrophobic phase is glassy (viscosity > 10^{12} Pa s) at RHs below 95%, with possible implications for heterogeneous reaction kinetics and cloud formation in the atmosphere. Using a kinetic multi-layer model (KM-GAP), we investigated the effect of two phases on the atmospheric lifetime of brown carbon within BBOA, which is a climate-warming agent. We showed that the presence of two phases can increase the lifetime of brown carbon in the planetary boundary layer and polar regions compared to previous modelling studies. Hence, liquid-liquid phase separation can lead to an increase in the predicted warming effect of BBOA on climate.

Introduction:

Smoke particles generated by the burning of biomass consist mainly of organic aerosol, referred to as biomass burning organic aerosol (BBOA) (1). For example, smoke sampled from wildfires in western USA was composed of > 90% BBOA (2, 3). BBOA represents the largest global contributor of organic aerosol emitted directly to the atmosphere (4), and the mass of emitted BBOA is expected to rise in the future due to increased prevalence of forest fires as a result of a warming world (5–7). BBOA influences the climate by scattering or absorbing solar radiation or by acting as nuclei of cloud droplets and possibly ice particles (1, 8). It contains a large amount of organic molecules that absorb UV and visible light, known as brown carbon (BrC), which leads to a warming of the earth-atmospheric system (9–12). While in the atmosphere, BrC can become oxidized by ozone or other atmospheric oxidants, eventually causing BBOA to become less absorbing with a weaker climatic impact (13–18). Despite the importance of BBOA, our understanding of the physical and chemical properties of BBOA particles is limited, leading to uncertainties in its impact on the global radiation budget.

The viscosity and the phase behavior, i.e. the number and types of phases present in a particle, are properties of BBOA that are expected to impact several climate-relevant processes. For example, phase separation and a high viscosity are properties that could lead to kinetic limitations on heterogeneous reactions (19–23), which could dictate the lifetime of BrC in BBOA and its warming effect on the climate (24). A low surface tension organic phase at the exterior of a particle with an aqueous-core can increase the particle's ability to act as a cloud condensation nucleus, thus affecting cloud formation and precipitation (25, 26). In addition, some studies have suggested that particles in a glassy state (viscosity > 10^{12} Pa s) could possibly act as heterogenous nuclei for the formation of ice clouds (27–32), thereby influencing the climate.

Previous studies have investigated the phase behavior of some types of atmospheric aerosol particles, such as mixtures of secondary organic aerosol with inorganic salts and mixtures of secondary organic aerosol with hydrocarbon-like organic aerosol (33–35). However, the phase behavior of primary BBOA remains understudied and unresolved. Models simulating the microphysics, chemical evolution, concentration or radiative properties of wildfire smoke typically assume that BBOA comprises only a single phase (24, 36–38). On the other hand, Jahn et al. identified that some sampled BBOA particles exhibited an organic shell coating an organic core using transmission electron microscopy images (39), with the caveat that the vacuum conditions required for this type of microscopy may affect the particle morphology. In addition, bulk-phase liquid tar condensates generated from high-temperature wood distillation were reported to have separated into a water-soluble and non-soluble oily phase (40, 41), although it is not known whether phase separation would occur in particles containing this material after equilibration with ambient RH. To our knowledge no study has yet explicitly shown liquid-liquid phase separation (LLPS) in BBOA particles for troposphere temperatures and RH conditions. Studies of BBOA phase behavior as a function of RH are vital, since the RH can vary considerably throughout the atmosphere and the RH controls the water content in particles, which can influence the phase behavior (42–44).

The viscosity of the water-soluble component of BBOA (generated by extracting BBOA with water) has been measured previously and was shown to depend strongly on the RH (24). However, the water-soluble component neglects the low-polarity compounds in BBOA that may significantly affect the viscosity of the total aerosol. Using a parameterization and high-resolution mass spectra of BBOA, DeRieux et al. predicted that the viscosity of BBOA is strongly dependent on RH and greater than 10^4 Pa s under dry conditions (45). However, these results had a high degree of uncertainty and were based on the assumption that BBOA contained a single phase. In addition, researchers often assume BBOA is in equilibrium with the gas phase in chemical transport models, implying a low viscosity (46, 47). No previous studies have measured the RH-dependent viscosity of the total BBOA. Furthermore, if BBOA undergoes LLPS then the viscosity of each individual phase must be measured independently.

In this work, we generated BBOA from smoldering pine in a controlled laboratory furnace. We studied the phase-behavior of the sampled primary BBOA using fluorescence microscopy and showed that BBOA particles comprise two phases (an outer hydrophobic phase and an inner hydrophilic phase) for a wide range of RH values relevant for the atmosphere. Using a photobleaching method, we showed that that the two phases possess very different RH-dependent viscosities. Using these results, we implement a kinetic multi-layer model of gas-particle interactions (KM-GAP) to demonstrate how liquid-liquid phase separation and viscosity of the BBOA can significantly affect the lifetime of BrC in the atmosphere and to highlight the need to include the phase behavior and viscosity of BBOA in calculations of the Earth's radiative balance.

Results

Phase behavior of BBOA as a function of RH

We generated BBOA particles by heating pine wood to 400 °C in a quartz furnace tube leading to smoldering combustion only (no flaming). The resulting BBOA was sampled onto glass slides coated with a hydrophobic and oleophobic coating for a high contact angle between particles and substrate. The RH-dependent phase behavior was then observed by placing the slide into a flow cell with temperature and RH control coupled to a widefield fluorescence microscope.

Widefield fluorescence microscopy images of pine BBOA particles showed two non-crystalline phases at all values of RH studied, as the humidity was ramped from low to high RH at 293 K (Fig. 1a). A

shell represents one organic phase and the central core is a second organic phase. Hereon we refer to the inner as the hydrophilic phase since it swelled with increasing RH. We refer to the outer phase as the hydrophobic phase since both its volume and viscosity (see below) were insensitive to the RH. The existence of multiple phases in BBOA particles is consistent with previous reports that show BBOA comprise chemical compounds with a broad range of polarities (48). Both phases are visible under the fluorescence microscope indicating that BrC is present in both phases. The chemical identity of the BrC in each phase is not known, although it is expected to comprise molecules formed in the breakdown of lignin and cellulose such as phenolic compounds and polycyclic aromatic hydrocarbons (40, 49–51).

Images of BBOA retrieved using a confocal laser scanning fluorescence microscope also clearly show the presence of two phases (Fig. 1b). The image in the y-z plane shows a partial ellipsoid (contact angle 125 °) within a spherical calotte (contact angle 72 °). Due to the contact angles of the two phases with the glass slide, the outer phase is either very thin or not continuous at the top of the BBOA particle (less than the resolution of the microscope). Similar morphologies have been observed for phase-separated particles deposited on substrates (52). As the particles in this work are deposited on substrates, the resulting morphology is influenced by the glass slide. Atmospheric particles that contain two phases are expected to exhibit a core-shell or partially-engulfed morphology when suspended in the atmosphere (44, 53, 54). Previous work has shown that particles deposited on hydrophobic substrates with morphologies similar to those shown here have core-shell morphologies when levitated in the gas phase (54), however, experiments are needed to confirm this for BBOA.

The volume percentage of the hydrophilic inner and hydrophobic outer phases was estimated using the 3D images of three separate BBOA particles at an RH of 58 ± 2 RH % (e.g. in Fig. 1b) to be 51 ± 5 % hydrophilic phase and 49 ± 5 % hydrophobic phase, for the 400 °C smoldering temperature. This ratio may be dependent upon the combustion conditions, as the chemical composition of BBOA has been shown to be dependent upon variables such as the fuel type, whether smoldering or flaming combustion occurred (55–57), and the combustion temperature, which can range from roughly 200 °C to > 700 °C (58). In this work we have resolved two phases in particles down to a size of ~ 6 µm, resulting from LLPS (Fig. S1). Previous work suggests that LLPS may be suppressed at particle diameters < 40 nm due to finite size effects (59) and hence, we expect the core-shell morphology to exist for BBOA particles larger than 40 nm, although further experiments are required to confirm this.

Viscosity of the individual phases at a range of tropospheric conditions

To quantify the viscosity within the two separate BBOA phases, we measured the diffusion coefficients of large dye molecules (Rhodamine-6G, hereon referred to as R6G) through the phases as a function of RH and converted the diffusion coefficients into viscosity using the Stokes-Einstein relation (60). The Stokes-Einstein relation has been shown to be a valid conversion between diffusion coefficients and viscosity for organic-water matrices when the hydrodynamic radius of the diffusing molecules under investigation (here the R6G dye molecules) is greater than or equal to the mean hydrodynamic radius of the surrounding matrix (61–63). For our experiments, the hydrodynamic radius of the diffusing dye molecules of 5.89 Å (64) is greater than the predicted mean hydrodynamic radius of the surrounding BBOA matrix of 4.23 Å (24), based on previous predictions of the average molar mass of BBOA being 248 g mol^{-1} (49) and a density of 1.3 g cm^{-3} (65, 66) and an assumed spherical geometry of BBOA molecules.

The diffusion coefficients of R6G through the BBOA phases were measured using rectangular fluorescence recovery after photobleaching (rFRAP) (67, 68). First, a phase-separated BBOA film (~30 µm thick) containing trace amounts of R6G dye deposited on a glass slide was imaged using a confocal laser scanning fluorescence microscope, and regions of interest containing either the hydrophilic or hydrophobic phase were selected. Following a period of photobleaching of a central rectangular region with the scanning laser, images were taken periodically to track the fluorescence recovery in the bleached region, and from the recovery time, the diffusion coefficient of the R6G was determined. An example of a typical rFRAP experiment is provided in the supplementary material (Fig. S4).

The measured diffusion coefficients of R6G through the two BBOA phases measured using rFRAP as a function of RH at 293 K are reported in Fig. 2a (left axis), with the derived viscosity reported on the right axis. Throughout the entire RH range studied, the hydrophobic phase exhibits a constant viscosity of 10^2 Pa s within the degree of experimental uncertainty. This is roughly the viscosity of ketchup. On the other hand, the viscosity of the hydrophilic phase is strongly dependent on the RH, decreasing from 10^3 Pa s (similar to peanut butter) to less than 10^0 Pa s (that of clear honey) between RHs of 10% and 75%. The decreasing viscosity with increasing RH of the hydrophilic phase is expected since increasing RH leads to water uptake and a corresponding decrease in the viscosity of hydrophilic and highly viscous particles and films, a process known as plasticization (69, 70). To parameterize the viscosity of the two BBOA phases as a function of RH, we fit our data to an Arrhenius mixing rule (Section S2). This expression has been used in the past to successfully describe the RH-dependent viscosity of a range of aerosol compositions (24, 71). The Arrhenius fit to the data (lines in Fig. 2a) shows that at 293 K and high RH conditions the viscosity of the hydrophobic phase can be up to five orders of magnitude greater than the hydrophilic phase.

The temperature and RH in the troposphere can vary from approximately 200 K to 300 K and 10% to 100%. To parameterize the measurements of viscosity of the two phases in BBOA as a function of both RH and temperature, we combine the Arrhenius mixing rule expression with the Vogel-Fulcher-Tamman equation (Section S2). The temperature- and RH-dependent viscosities of the hydrophilic and hydrophobic phases in BBOA are reported in Fig. 2b and c. The viscosity of the hydrophilic phase shows a strong dependence on both the temperature and the RH, similar to the viscosity of the water soluble component of BBOA and secondary organic aerosol observed in other studies (24, 72–74). In sharp contrast, the viscosity of the hydrophobic phase is largely independent of the RH between values from 0 to approximately 95% at all temperatures. For temperatures between 293 K and 230 K, the hydrophobic phase is semisolid (viscosity > 10^2 Pa s) for all RH values below 95%, and for colder temperatures the hydrophobic state is glassy (viscosity > 10^{12} Pa s) at all RHs below 95%. Although previous studies have identified that atmospheric aerosol can exhibit glassy states at low temperatures and low RHs (69, 71, 74), to our knowledge this is the first study to show glassy states could be present in atmospheric aerosol at RHs as high as 95%. Furthermore, for numerous temperatures and at higher RH conditions, the viscosity of the hydrophobic phase can be many orders of magnitude higher than that of the hydrophilic phase, as evidenced in the plot of the viscosity difference between the two phases in Figure S2.

To estimate the zonally-averaged viscosity of the two phases of a BBOA particle in the troposphere, we implemented the parameterizations for temperature- and RH-dependent viscosity for each phase into the mean annual tropospheric RH and temperature profiles from the Modern-Era Retrospective analysis for Research and Applications, Version 2 (MERRA-2, (75)). The underlying distribution of the RH and temperature as a function of altitude and latitude are reported in Fig. S3. Shown in Figure 3 are the zonally-averaged viscosities resulting from this implementation. Based on these zonally-averaged viscosities, the hydrophilic phase is mostly liquid-like (<10^2 Pa s) below an altitude of 2 km, mostly in a semi-solid state between 2 and 9 km and in a glassy state above that (Fig. 3a). Conversely, the hydrophobic phase is mostly semi-solid below 2 km, a semi-solid or glassy state between 2 and 9 km, and glassy above that (Fig. 3b).

The difference in viscosity for the two phases (Fig. 3c) highlights global regions wherein the prevalence of LLPS may be of greater importance for atmospheric process. For many regions of the troposphere, including much of the planetary boundary layer (<1 km altitude) and in polar regions at all altitudes, there is between two and six orders of magnitude difference between the viscosities of the two phases of BBOA (Fig. 3c). For these conditions, the higher viscosity of the outer hydrophobic phase could significantly impact atmospheric processes, as discussed below.

Atmospheric implications.

Implications for liquid- and ice-cloud nucleation.

Ice nucleation in the atmosphere has a complex impact on the climate, altering the way clouds interact with solar radiation and hence modifying Earth's radiative budget, as well as affecting precipitation and cloud lifetimes (76–78). The role that organic aerosol play in the nucleation of ice is still an active area of debate (27, 28, 79), but some studies suggest that glassy organic aerosol (at

least single-component glassy aerosol) can act as a heterogeneous nuclei for ice clouds (27, 29–32). Ice nucleation arising from wildfire smoke plumes in the free troposphere has been observed (80), with the mechanism thought to be from soot (from flaming combustion) or from inorganic components and minerals naturally present in biomass (81, 82). As the outer shell of BBOA can exhibit viscosities commensurate with those of a glass even at high RHs, we speculate that the organic aerosol component of biomass burning plumes might represent an additional mechanism towards ice nucleation, with resulting climatic impacts. In terms of liquid cloud droplet nucleation, the presence of the hydrophobic outer shell in a BBOA particle would also likely reduce the particle's surface tension compared to if it were to comprise only a well-mixed single phase (25, 26). Hence, this phase separation behavior could increase the ability of BBOA to nucleate liquid cloud droplets (26, 43, 83), thereby indirectly affecting Earth's interaction with solar radiation.

Implications for BrC whitening

As a case study to highlight the importance of LLPS and viscosity of BBOA, we focus on the heterogeneous reaction kinetics between ozone and BrC within BBOA. The BrC within BBOA can absorb solar radiation and lead to warming of the earth-atmospheric system (11, 12). In the atmosphere, heterogenous reactions between ozone and BrC can lead to whitening (13, 14). Recently, Schnitzler et al. showed that the whitening rate of BrC by ozone was strongly dependent upon the viscosity, with lifetimes of BrC (τ_{BrC}) in the upper troposphere extending to more than one day and τ_{BrC} in the planetary boundary layer less than one day (24). However, this study only investigated the properties of the water-soluble component of BBOA, which is analogous to studying only the hydrophilic phase in this work. Here we study how both LLPS and viscosity may impact the atmospheric lifetime of BrC in BBOA.

We apply the kinetic multi-layer model of gas-particle interactions (KM-GAP) to simulate the reactive uptake of ozone into a 150 nm diameter BBOA particle for three different cases: 1) a particle comprising only the hydrophobic phase; 2) a particle comprising only the hydrophilic phase, similar to studies that investigate only the water-soluble component of BBOA samples; and 3) a particle that has undergone LLPS to consist of an inner hydrophilic core and an outer hydrophobic shell. The KM-GAP model is described in more detail in the Material and Methods section, and elsewhere (84, 85). The model explicitly treats mass transport including gas-phase O_3 diffusion, adsorption and surface-to-bulk transport of O_3, and bulk diffusion of BrC and O_3 within the core and shell phase as well as multiphase reactions between O_3 and BrC.

The modelling results at 293 K show that in a particle consisting of only the hydrophilic phase, the atmospheric lifetime (e-folding time, τ_{BrC}) of BrC is strongly dependent upon the RH, decreasing from 20 h to 5 h between 40 and 95% RH (Fig. 4a). These results are consistent with the whitening results for the water-soluble component of BrC reported by Schnitzler et al. (24). At 10% RH, τ_{BrC} for the hydrophilic particle is ~ 40 h, arising from the low experimentally-derived value for D_{R6G} at this RH for the hydrophilic phase in Fig. 2a. However, for a BBOA particle that has undergone LLPS, τ_{BrC} remains reasonably constant at approximately 1 day for RH 0 – 95% (Fig. 4a), following a similar RH-dependency to the pure-hydrophobic case. The difference between a particle consisting of only the hydrophilic phase and a particle that has undergone LLPS illustrates how the presence of the hydrophobic outer phase on the outside of a particle can drastically change the whitening rates by acting as a kinetic barrier to the uptake of ozone. Thus, LLPS can lengthen the potential warming effect of BrC compared to models or experiments that only consider the water-soluble component of BBOA.

To further emphasize the importance of including the hydrophobic phase at the surface of BBOA particles, we extend the KM-GAP model to simulate τ_{BrC} for three locations within the planetary boundary layer (specifically at 0.5 km altitude and 0°, 40° and 80° latitude; see square symbols in Fig. 3c). The KM-GAP model shows that τ_{BrC} for a phase-separated particle is a factor of 3.0, 4.4, and 50 times larger than a hydrophilic-only particle at these three locations (Fig. 4b). In addition, a two-phase core-shell particle of BBOA will have an atmospheric lifetime of 0.8, 1.7 and 12 days at these three locations within the planetary boundary layer. In contrast, it has previously been assumed that τ_{BrC} is 1 day everywhere in the planetary boundary layer when predicting the climatic effects of BBOA (24, 86, 87). We conclude that the total BBOA aerosol including the presence of liquid-liquid phase separation needs to be considered when estimating τ_{BrC}. Particularly in the planetary boundary layer and at polar

regions, the lifetime of BrC and hence its warming effect can be much larger than assumed in previous modelling studies.

Materials and methods

Woodsmoke aerosol sample collection

BBOA samples were produced through the smoldering of pine wood with a methodology based on that described by Kim et al. (57). Untreated pine wood from a hardware store were cut into strips (~ 20 x 2 x 2 mm) and 1.2 g total mass of the strips were placed lengthwise inside a quartz flow tube (inner diameter 37 mm, outer diameter 40 mm, length 1100 mm). Pressurised room air from a compressor (Oil-free 380 Series, Thomas, Sheboygan USA) was passed through the tube at a flow rate of 2 l min^{-1}, controlled by a mass flow controller (MKS, Andover USA). A ceramic tubular heater (length 150 mm, Watlow, St. Louis USA) fitting around the flow tube moved along the length of the flow tube in the direction of the air flow at a speed of 10 mm min^{-1}, propelled by a custom-built motorized track, enabling a steady and controlled aerosol flow from the smoldering phase of combustion only. The heating temperature was controlled by varying the heater voltage, with 65 V used to access a temperature of 400 °C, as calibrated by a K-type thermocouple. Constraining the experimental conditions to feature only smoldering rather than flaming conditions led to no visible evidence of black carbon present in the particles (Fig. 1 and S1).

The woodsmoke aerosol was subjected to 10:1 dilution with HEPA-filtered air into a sampling chamber (4.75 m^3) out of which the aerosol was sampled onto glass slides. For microscopy experiments (e.g. Fig. 1 and S1), BBOA was sampled onto 12 mm glass slides using a MOUDI-II impactor (120R using stage 7, TSI, Minnesota USA), cut size 0.32 µm, serviced by a pump (Varian, Lexington USA) running at 30 l min^{-1} for ~ 5 minutes. Collection times were long enough so that sub-micron BBOA particles deposited and agglomerated on the slides to form super-micron BBOA particles. Slides were pre-coated with FluoroPel-800 (Cytonix, Beltsville USA) to have a hydrophobic and oleophobic surface for higher particle contact angles and improved imaging. Experimental details about the microscopy imaging of particles is given in Section S3.1. Samples for rFRAP measurements were collected onto 22 mm siliconized slides with a slit impactor (Sioutas, SKC, Pennsylvania USA) with cut size 0.25 µm serviced by the pump running at 9 l min^{-1}. For rFRAP, thin films of sample are required, so the glass slides were not coated with Fluoropel-800 to allow for a lower contact angle. Samples were sealed in a Petri dish and stored in a freezer until use. A detailed schematic of the woodsmoke generation system is presented in Fig. S7.

Diffusion coefficients and viscosity

Diffusion coefficients of Rhodamine-6G dye (R6G) through the different phases of BBOA (D_{R6G}) were measured using rectangular Fluorescence Recovery After Photobleaching (rFRAP) (67, 68). Briefly, films of sampled BBOA with additional trace amounts of R6G were imaged using a confocal laser scanning fluorescence microscope, and a central rectangular region was photobleached. The RH-dependent diffusion coefficient of R6G was calculated from the timescale through which the fluorescence intensity within the bleached region recovered, arising from diffusion of the dye through the BBOA film. This is described in more detail in the Supplementary Materials section (Section S3.2). The diffusion coefficients of R6G were then used to calculate the viscosity of the BBOA phases using the Stokes-Einstein relation (60).

Kinetic modeling

The kinetic multilayer model of gas-particle interactions in aerosols and clouds (KM-GAP) was used to simulate the uptake of ozone by BBOA particles and to determine the lifetime (i.e. e-folding timescale) of BrC within BBOA due to oxidative aging by ozone. The full description of this model can be found in (Shiraiwa ACP 2012, Shiraiwa PCCP 2013, refs 69 and 70), but a brief description is given here as well as a description of the updates for this implementation. KM-GAP consists of multiple model layers including a gas phase, a near-surface gas phase, a sorption layer, a near-surface bulk layer, and a number of bulk layers. KM-GAP explicitly treats the processes of gas-phase diffusion, adsorption and desorption, surface-to-bulk transport and bulk diffusion within the particle. In this work, for phase-separated particles, bulk mass transport includes transport between layers within each phase as well as transport between the two phases. Because the simulation scenarios included a hydrophilic core at very low RH, the original KM-GAP model was updated to include multiple core

layers to account for potential diffusion limitations. Here we use 10 total layers in all simulations. In the phase-separated cases, these are divided as 5 layers in the shell phase and 5 layers in the core phase. Chemical reactions of ozone and BrC were treated in both phases. Kinetic parameters used in the simulations are given in Table S2. The product of the reaction between BrC and ozone was assumed to have the same properties as the BrC and the rest of the particle consists of non-reactive and non-volatile species. To quantify the lifetime of BrC, τ_{BrC}, we use the e-folding timescale, which represents the time it takes for the amount of BrC to reach 1/e of its final value relative to its initial value in the whole particle.

For the simulations, BrC was assumed to be capable of transporting between the two phases as describe in Shiraiwa, PCCP 2013. The justification for this assumption is discussed in the supplementary material (section S4). The initial molar concentration of the two different condensed phases was assumed to be equal, and the activity coefficients of BrC in both condensed phases was assumed to be 1, resulting in equal concentrations of BrC in both condensed phases at equilibrium. However, we also varied this assumption, and found the lifetime of BrC were not sensitive to the relative concentrations of BrC in the two phases (sections S3.1).

Acknowledgements
This work was supported by the Natural Sciences and Engineering Research Council of Canada through grant RGPIN/ 04441-2016 (FKAG, NGAG, SN and AKB). SK acknowledges support from the Canadian Foundation for Innovation (CFI) and BC Knowledge Development Fund (BCKDF). M. Sh acknowledges funding from U.S. National Science Foundation (AGS-1654104). The Scientific colour map Batlow from Crameri et al. (Nat. Commun. 11, 1–10 (2020) is used in this study to prevent visual distortion of the data and exclusion of readers with colour-vision deficiencies. This work was conducted on the traditional, ancestral and unceded territory of the Musqueam Nation.

Figures:

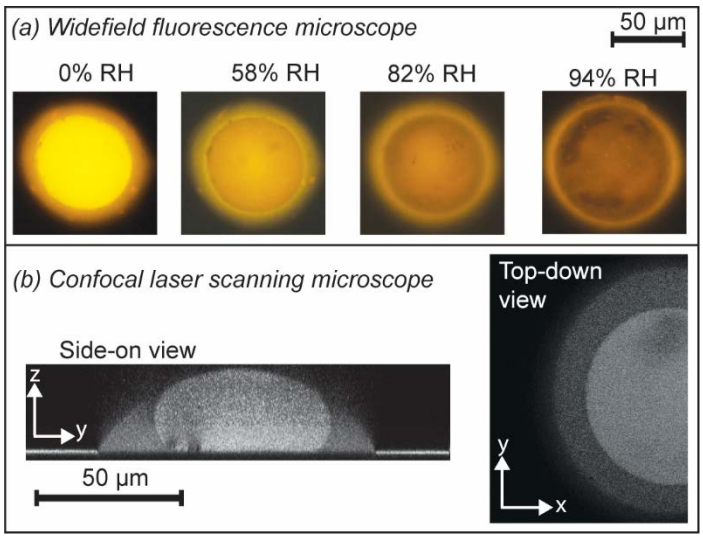

Figure 1: (a) Widefield fluorescence microscopy images of pine BBOA during an RH-increase experiment (top-down view), demonstrating that the BBOA exists as two liquid phases. (b) Laser scanning images using a confocal fluorescence microscope with a z-stack at 58% RH. The top-down image was taken approximately 1/3 of the way up through the particle. All particles were deposited on a hydrophobic and oleophobic glass slide.

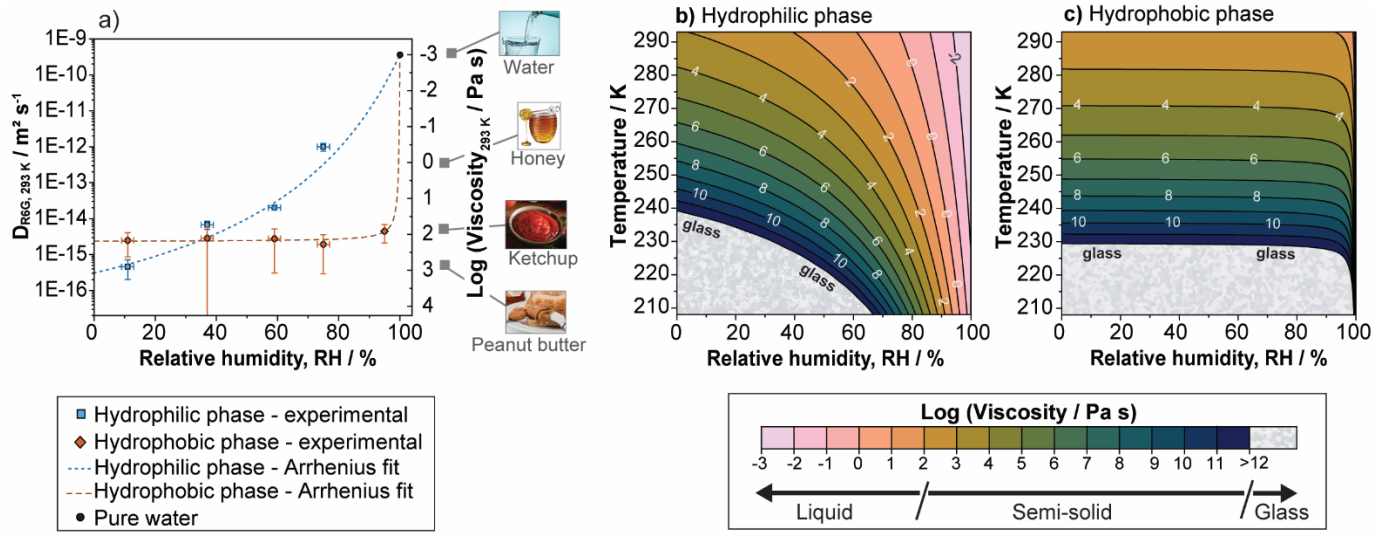

Figure 2: a) The diffusion coefficient of Rhodamine-6G dye (D_{R6G}, left axis) through the hydrophilic and hydrophobic liquid phases of phase-separated pine BBOA as a function of RH at 293 K. The viscosity of the two phases is retrieved using the Stokes Einstein conversion (right axis) and compared to that of honey, ketchup and peanut butter (69)*. Lines represent fits using an Arrhenius mixing rule (Equation S1) The black circle at 100% RH represents the diffusion of the dye in pure water at 293 K. b) The log(viscosity) of the hydrophilic phase and (c) the hydrophobic phase in BBOA as a function of temperature and RH as predicted by the Vogel-Fulcher-Tamman (VFT) equation (Equation S2). The grey region represents the onset of the glass state (viscosity > 10^{12} Pa s) for which the data is cut off as these viscosities are not modelled well by the VFT equation.*

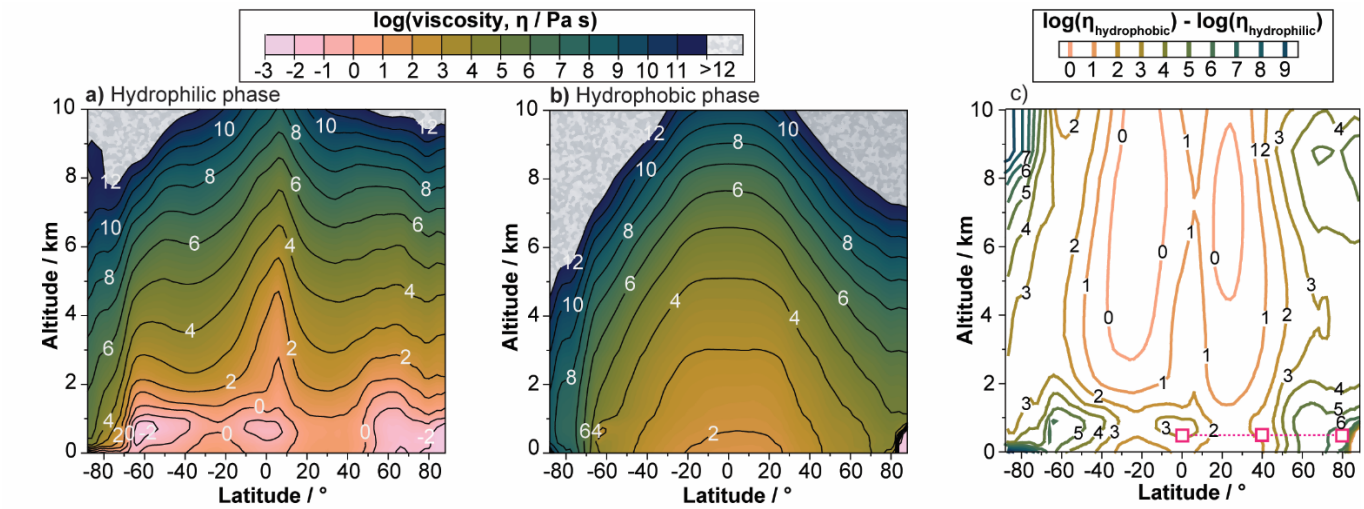

Figure 3: The predicted viscosity of the (a) hydrophilic phase and (b) hydrophobic phase of BBOA, zonally averaged as a function of latitude and altitude in the troposphere. c) The difference in log(viscosity) between the hydrophilic and the hydrophobic phases at each atmospheric location. The horizontal pink line and squares correspond to 0.5 km altitude, which are conditions explored in Fig. 4b.

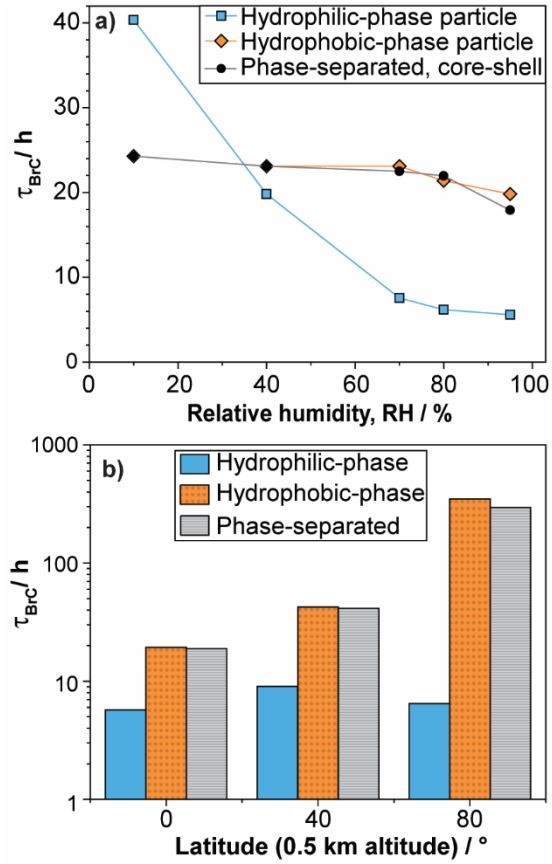

Figure 4: a) The lifetime of reactive BrC in the atmosphere (τ_{BrC}) due to oxidative aging by O_3 as a function of RH at 293 K, modelled using KM-GAP and assuming one of three different cases: 1) particles comprise only the hydrophobic phase (orange), 2) particles comprise only the hydrophilic phase (blue) and 3) particles consist of two phases in a core-shell morphology with a hydrophilic core and a hydrophobic shell. b) The atmospheric lifetime of reactive BrC due to oxidative aging by O_3, for each modeling case, at a mean altitude of 0.5 km at three different latitudes, corresponding to the pink square locations in Fig. 3c. The RH and temperatures are 87.5% and 295.2 K, 71.9% and 283.9 K, and 96.1% and 261.4 K for the latitudes of 0°, 40° and 80° respectively. The underlying KM-GAP modelling results of the decay in reactive BrC concentration are reported in the Supplementary material Fig. S9 and S10 for panels a and b, respectively.

References

1. J. S. Reid, *et al.*, A review of biomass burning emissions part II: intensive physical properties of biomass burning particles. *Atmos. Chem. Phys.* **5**, 799–825 (2005).
2. X. Liu, *et al.*, Airborne measurements of western U.S. wildfire emissions: Comparison with prescribed burning and air quality implications. *J. Geophys. Res.* **122**, 6108–6129 (2017).
3. A. A. May, *et al.*, Aerosol emissions from prescribed fires in the United States: A synthesis of laboratory and aircraft measurements. *J. Geophys. Res.* **119**, 11,826–11,849 (2014).
4. T. C. Bond, *et al.*, Bounding the role of black carbon in the climate system: A scientific assessment. *J. Geophys. Res. Atmos.* **118**, 5380–5552 (2013).
5. Q. Sun, *et al.*, Global heat stress on health, wildfires, and agricultural crops under different levels of climate warming. *Environ. Int.* **128**, 125–136 (2019).
6. P. E. Dennison, S. C. Brewer, J. D. Arnold, M. A. Moritz, Large wildfire trends in the western United States, 1984–2011. *Geophys. Res. Lett.* **41**, 2928–2933 (2014).
7. J. G. Canadell, *et al.*, Multi-decadal increase of forest burned area in Australia is linked to climate change. *Nat. Commun.* **12** (2021).
8. A. L. Hodshire, *et al.*, Aging Effects on Biomass Burning Aerosol Mass and Composition: A Critical Review of Field and Laboratory Studies. *Environ. Sci. Technol.* **53**, 10007–10022 (2019).
9. J. Liu, *et al.*, Brown carbon in the continental troposphere. *Geophys. Res. Lett.* **41**, 2191–2195 (2014).
10. H. Brown, *et al.*, Biomass burning aerosols in most climate models are too absorbing. *Nat. Commun.* **12** (2021).
11. R. Saleh, From Measurements to Models: Toward Accurate Representation of Brown Carbon in Climate Calculations. *Curr. Pollut. Reports* **6**, 90–104 (2020).
12. C. E. Chung, V. Ramanathan, D. Decremer, Observationally constrained estimates of carbonaceous aerosol radiative forcing. *Proc. Natl. Acad. Sci. U. S. A.* **109**, 11624–11629 (2012).
13. R. F. Hems, E. G. Schnitzler, C. Liu-Kang, C. D. Cappa, J. P. D. Abbatt, Aging of Atmospheric Brown Carbon Aerosol. *ACS Earth Sp. Chem.* **5**, 722–748 (2021).
14. E. C. Browne, *et al.*, Effect of heterogeneous oxidative aging on light absorption by biomass burning organic aerosol. *Aerosol Sci. Technol.* **53**, 663–674 (2019).
15. B. Sumlin, *et al.*, Diel cycle impacts on the chemical and light absorption properties of organic carbon aerosol from wildfires in the western United States. *Atmos. Chem. Phys.* **21**, 11843–11856 (2021).
16. C. L. Li, *et al.*, Formation of Secondary Brown Carbon in Biomass Burning Aerosol Proxies through NO3 Radical Reactions. *Environ. Sci. Technol.* **54**, 1395–1405 (2020).
17. J. P. S. Wong, *et al.*, Atmospheric evolution of molecular-weight-separated brown carbon from biomass burning. *Atmos. Chem. Phys.* **19**, 7319–7334 (2019).
18. H. Forrister, *et al.*, Evolution of brown carbon in wildfire plumes. *Geophys. Res. Lett.* **42**, 4623–4630 (2015).
19. M. Kuwata, S. T. Martin, Phase of atmospheric secondary organic material affects its reactivity. *Proc. Natl. Acad. Sci. U. S. A.* **109**, 17354–17359 (2012).
20. S. S. Steimer, M. Lampimäki, E. Coz, G. Grzinic, M. Ammann, The influence of physical state on shikimic acid ozonolysis: A case for in situ microspectroscopy. *Atmos. Chem. Phys.* **14**, 10761–10772 (2014).
21. Y. You, *et al.*, Images reveal that atmospheric particles can undergo liquid-liquid phase separations. *Proc. Natl. Acad. Sci. U. S. A.* **109**, 13188–13193 (2012).
22. S. Zhou, *et al.*, Multiphase reactivity of polycyclic aromatic hydrocarbons is driven by phase separation and diffusion limitations. *Proc. Natl. Acad. Sci. U. S. A.* **116**, 11658–11663 (2019).
23. Y. Zhang, *et al.*, Effect of the Aerosol-Phase State on Secondary Organic Aerosol Formation from the Reactive Uptake of Isoprene-Derived Epoxydiols (IEPOX). *Environ. Sci. Technol. Lett.* **5**, 167–174 (2018).
24. E. G. Schnitzler, *et al.*, Rate of atmospheric brown carbon whitening governed by environmental conditions. *Proc. Natl. Acad. Sci.* **119**, 2205610119 (2022).
25. J. Ovadnevaite, *et al.*, Surface tension prevails over solute effect in organic-influenced cloud droplet activation. *Nature* **546**, 637–641 (2017).
26. P. Liu, *et al.*, Resolving the mechanisms of hygroscopic growth and cloud condensation nuclei activity for organic particulate matter. *Nat. Commun.* **9** (2018).
27. M. J. Wolf, *et al.*, A biogenic secondary organic aerosol source of cirrus ice nucleating particles. *Nat. Commun.* **11** (2020).

28. D. A. Knopf, P. A. Alpert, B. Wang, The Role of Organic Aerosol in Atmospheric Ice Nucleation: A Review. *ACS Earth Sp. Chem.* **2**, 168–202 (2018).
29. A. D. James, *et al.*, Nucleation of nitric acid hydrates in polar stratospheric clouds by meteoric material. *Atmos. Chem. Phys.* **18**, 4519–4531 (2018).
30. B. J. Murray, *et al.*, Heterogeneous nucleation of ice particles on glassy aerosols under cirrus conditions. *Nat. Geosci.* **3**, 233–237 (2010).
31. G. P. Schill, M. A. Tolbert, Heterogeneous ice nucleation on phase-separated organic-sulfate particles: Effect of liquid vs. glassy coatings. *Atmos. Chem. Phys.* **13**, 4681–4695 (2013).
32. K. Ignatius, *et al.*, Heterogeneous ice nucleation of viscous secondary organic aerosol produced from ozonolysis of alpha-pinene. *Atmos. Chem. Phys.* **16**, 6495–6509 (2016).
33. M. A. Freedman, Liquid-Liquid Phase Separation in Supermicrometer and Submicrometer Aerosol Particles. *Acc. Chem. Res.* **53**, 1102–1110 (2020).
34. Y. Huang, *et al.*, Coexistence of three liquid phases in individual atmospheric aerosol particles. *PNAS* **118**, e2102512118 (2021).
35. U. K. Krieger, C. Marcolli, J. P. Reid, Exploring the complexity of aerosol particle properties and processes using single particle techniques. *Chem. Soc. Rev.* **41**, 6631–6662 (2012).
36. T. B. Zhuravleva, I. M. Nasrtdinov, I. B. Konovalov, N. A. Golovushkin, M. Beekmann, Impact of the atmospheric photochemical evolution of the organic component of biomass burning aerosol on its radiative forcing efficiency: A box model analysis. *Atmosphere (Basel).* **12** (2021).
37. A. Akherati, *et al.*, Dilution and photooxidation driven processes explain the evolution of organic aerosol in wildfire plumes. *Environ. Sci. Atmos.* **2**, 1000–1022 (2022).
38. D. Patoulias, E. Kallitsis, L. Posner, S. N. Pandis, Modeling biomass burning organic aerosol atmospheric evolution and chemical aging. *Atmosphere (Basel).* **12**, 1–18 (2021).
39. L. G. Jahn, L. G. Jahl, B. B. Bowers, R. C. Sullivan, Morphology of Organic Carbon Coatings on Biomass-Burning Particles and Their Role in Reactive Gas Uptake. *ACS Earth Sp. Chem.* **5**, 2184–2195 (2021).
40. A. P. S. Hettiyadura, *et al.*, Chemical composition and molecular-specific optical properties of atmospheric brown carbon associated with biomass burning. *Environ. Sci. Technol.* **55**, 2511–2521 (2021).
41. C. Li, *et al.*, Dynamic changes in optical and chemical properties of tar ball aerosols by atmospheric photochemical aging. *Atmos. Chem. Phys.* **19**, 139–163 (2019).
42. Y. C. Song, *et al.*, Liquid-liquid phase separation and morphologies in organic particles consisting of α-pinene and β-caryophyllene ozonolysis products and mixtures with commercially available organic compounds. *Atmos. Chem. Phys.* **20**, 11263–11273 (2020).
43. L. Renbaum-Wolff, *et al.*, Observations and implications of liquid-liquid phase separation at high relative humidities in secondary organic material produced by α-pinene ozonolysis without inorganic salts. *Atmos. Chem. Phys.* **16**, 7969–7979 (2016).
44. K. Gorkowski, N. M. Donahue, R. C. Sullivan, Aerosol Optical Tweezers Constrain the Morphology Evolution of Liquid-Liquid Phase-Separated Atmospheric Particles. *Chem* **6**, 204–220 (2020).
45. W. S. W. DeRieux, *et al.*, Predicting the glass transition temperature and viscosity of secondary organic material using molecular composition. *Atmos. Chem. Phys.* **18**, 6331–6351 (2018).
46. A. B. M. Collow, *et al.*, An evaluation of biomass burning aerosol mass , extinction , and size distribution in GEOS using observations from CAMP 2 Ex. 16091–16109 (2022).
47. J. K. Kodros, *et al.*, Rapid dark aging of biomass burning as an overlooked source of oxidized organic aerosol. *Proc. Natl. Acad. Sci. U. S. A.* **117**, 33028–33033 (2020).
48. X. Jiang, *et al.*, Connecting the Light Absorption of Atmospheric Organic Aerosols with Oxidation State and Polarity. *Environ. Sci. Technol.* **56**, 12873–12885 (2022).
49. L. T. Fleming, *et al.*, Molecular composition and photochemical lifetimes of brown carbon chromophores in biomass burning organic aerosol. *Atmos. Chem. Phys.* **20**, 1105–1129 (2020).
50. B. B. Palm, *et al.*, Quantification of organic aerosol and brown carbon evolution in fresh wildfire plumes. *Proc. Natl. Acad. Sci. U. S. A.* **117**, 29469–29477 (2020).
51. A. Laskin, J. Laskin, S. A. Nizkorodov, Chemistry of Atmospheric Brown Carbon. *Chem. Rev.* **115**, 4335–4382 (2015).
52. V. G. Ciobanu, C. Marcolli, U. K. Krieger, U. Weers, T. Peter, Liquid-liquid phase separation in mixed organic/inorganic aerosol particles. *J. Phys. Chem. A* **113**, 10966–10978 (2009).
53. J. P. Reid, *et al.*, The morphology of aerosol particles consisting of hydrophobic and

hydrophilic phases: Hydrocarbons, alcohols and fatty acids as the hydrophobic component. *Phys. Chem. Chem. Phys.* **13**, 15559–15572 (2011).
54. M. Song, C. Marcolli, U. K. Krieger, D. M. Lienhard, T. Peter, Morphologies of mixed organic/inorganic/aqueous aerosol droplets. *Faraday Discuss.* **165**, 289–316 (2013).
55. L. Kam Chan, *et al.*, Relationship between the molecular composition, visible light absorption, and health-related properties of smoldering woodsmoke aerosols. *Atmos. Chem. Phys.* **20**, 539–559 (2020).
56. C. N. Jen, *et al.*, Speciated and total emission factors of particulate organics from burning western US wildland fuels and their dependence on combustion efficiency. *Atmos. Chem. Phys.* **19**, 1013–1026 (2019).
57. Y. H. Kim, *et al.*, Mutagenicity and lung toxicity of smoldering vs. Flaming emissions from various biomass fuels: Implications for health effects from wildland fires. *Environ. Health Perspect.* **126** (2018).
58. N. Gorbach, *et al.*, Simulation of Smoldering Combustion of Organic Horizons at Two Types of Boreal Forests with Lab-Heating Experiments. *SSRN Electron. J.* (2022) https:/doi.org/10.2139/ssrn.4202081.
59. M. B. Altaf, M. A. Freedman, Effect of Drying Rate on Aerosol Particle Morphology. *J. Phys. Chem. Lett.* **8**, 3613–3618 (2017).
60. Y. Chu, *et al.*, Viscosity of erythritol and erythritol-water particles as a function of water activity: New results and an intercomparison of techniques for measuring the viscosity of particles. *Atmos. Meas. Tech.* **11**, 4809–4822 (2018).
61. H. C. Price, J. Mattsson, B. J. Murray, Sucrose diffusion in aqueous solution. *Phys. Chem. Chem. Phys.* **18**, 19207–19216 (2016).
62. E. Evoy, S. Kamal, G. N. Patey, S. T. Martin, A. K. Bertram, Unified Description of Diffusion Coefficients from Small to Large Molecules in Organic–Water Mixtures. *J. Phys. Chem. A* **124**, 2301–2308.
63. E. Evoy, *et al.*, Predictions of diffusion rates of large organic molecules in secondary organic aerosols using the Stokes-Einstein and fractional Stokes-Einstein relations. *Atmos. Chem. Phys.* **19**, 10073–10085 (2019).
64. C. B. Müller, *et al.*, Precise measurement of diffusion by multi-color dual-focus fluorescence correlation spectroscopy. *Epl* **83**, 0–5 (2008).
65. J. Chen, *et al.*, A review of biomass burning: Emissions and impacts on air quality, health and climate in China. *Sci. Total Environ.* **579**, 1000–1034 (2017).
66. C. J. Hennigan, *et al.*, Chemical and physical transformations of organic aerosol from the photo-oxidation of open biomass burning emissions in an environmental chamber. *Atmos. Chem. Phys.* **11**, 7669–7686 (2011).
67. H. Deschout, *et al.*, Straightforward FRAP for quantitative diffusion measurements with a laser scanning microscope. *Opt. Express* **18**, 22886–22905 (2010).
68. Y. Chenyakin, *et al.*, Diffusion coefficients of organic molecules in sucrose-water solutions and comparison with Stokes-Einstein predictions. *Atmos. Chem. Phys.* **17**, 2423–2435 (2017).
69. T. Koop, J. Bookhold, M. Shiraiwa, U. Pöschl, Glass transition and phase state of organic compounds: Dependency on molecular properties and implications for secondary organic aerosols in the atmosphere. *Phys. Chem. Chem. Phys.* **13**, 19238–19255 (2011).
70. S. O'Meara, D. O. Topping, G. McFiggans, The rate of equilibration of viscous aerosol particles. *Atmos. Chem. Phys.* **16**, 5299–5313 (2016).
71. A. M. Maclean, *et al.*, Humidity-Dependent Viscosity of Secondary Organic Aerosol from Ozonolysis of β-Caryophyllene: Measurements, Predictions, and Implications. *ACS Earth Sp. Chem.* **5**, 305–318 (2021).
72. A. M. Maclean, *et al.*, Global Distribution of the Phase State and Mixing Times within 2 Secondary Organic Aerosol Particles in the Troposphere Based on 3 Room-Temperature Viscosity Measurements. *ACS Earth Sp. Chem.* **5**, 3458–3473 (2021).
73. K. J. Kiland, A. M. MacLean, S. Kamal, A. K. Bertram, Supplemental Information: Diffusion of Organic Molecules as a Function of Temperature in a Sucrose Matrix (a Proxy for Secondary Organic Aerosol). *J. Phys. Chem. Lett.* **10**, 5902–5908 (2019).
74. S. S. Petters, S. M. Kreidenweis, A. P. Grieshop, P. J. Ziemann, M. D. Petters, Temperature- and Humidity-Dependent Phase States of Secondary Organic Aerosols. *Geophys. Res. Lett.* **46**, 1005–1013 (2019).
75. T. S. Carter, *et al.*, Investigating Carbonaceous Aerosol and Its Absorption Properties From Fires in the Western United States (WE-CAN) and Southern Africa (ORACLES and CLARIFY). *J. Geophys. Res. Atmos.* **126**, 1–28 (2021).

76. P. J. DeMott, *et al.*, Predicting global atmospheric ice nuclei distributions and their impacts on climate. *Proc. Natl. Acad. Sci. U. S. A.* **107**, 11217–11222 (2010).
77. U. Lohmann, J. Feichter, Global indirect aerosol effects: a review. *Atmos. Chem. Phys.* **5**, 715–737 (2005).
78. T. Storelvmo, Aerosol Effects on Climate via Mixed-Phase and Ice Clouds. *Annu. Rev. Earth Planet. Sci.* **45**, 199–222 (2017).
79. S. Kasparoglu, *et al.*, Experimental Determination of the Relationship Between Organic Aerosol Viscosity and Ice Nucleation at Upper Free Tropospheric Conditions. *J. Geophys. Res. Atmos.* **127**, 1–20 (2022).
80. K. R. Barry, *et al.*, Observations of Ice Nucleating Particles in the Free Troposphere From Western US Wildfires. *J. Geophys. Res. Atmos.* **126**, 1–17 (2021).
81. L. G. Jahn, *et al.*, Biomass combustion produces ice-active minerals in biomass-burning aerosol and bottom ash. *Proc. Natl. Acad. Sci. U. S. A.* **117**, 21928–21937 (2020).
82. M. D. Petters, *et al.*, Ice nuclei emissions from biomass burning. *J. Geophys. Res. Atmos.* **114**, 1–10 (2009).
83. C. R. Ruehl, J. F. Davies, K. R. Wilson, An interfacial mechanism for cloud droplet formation on organic aerosols. *Science (80-.).* **351**, 1447–1450 (2016).
84. M. Shiraiwa, A. Zuend, A. K. Bertram, J. H. Seinfeld, Gas-particle partitioning of atmospheric aerosols: Interplay of physical state, non-ideal mixing and morphology. *Phys. Chem. Chem. Phys.* **15**, 11441–11453 (2013).
85. M. Shiraiwa, C. Pfrang, T. Koop, U. Pöschl, Kinetic multi-layer model of gas-particle interactions in aerosols and clouds (KM-GAP): Linking condensation, evaporation and chemical reactions of organics, oxidants and water. *Atmos. Chem. Phys.* **12**, 2777–2794 (2012).
86. T. S. Carter, *et al.*, Investigating Carbonaceous Aerosol and Its Absorption Properties From Fires in the Western United States (WE-CAN) and Southern Africa (ORACLES and CLARIFY). *J. Geophys. Res. Atmos.* **126** (2021).
87. X. Wang, *et al.*, Exploring the observational constraints on the simulation of brown carbon. *Atmos. Chem. Phys.* **18**, 635–653 (2018).